#22
4/29/80

SAND 79-1665
Unlimited Release

THERMAL CONDUCTIVITY OF ROCKSALT AND OTHER GEOLOGIC MATERIALS FROM THE SITE OF THE PROPOSED WASTE ISOLATION PILOT PLANT

J. N. Sweet and J. E. McCreight, 5824

F 2900-Q(3-80)

THERMAL CONDUCTIVITY OF ROCKSALT AND OTHER GEOLOGIC MATERIALS FROM THE SITE OF THE PROPOSED WASTE ISOLATION PILOT PLANT

J. N. Sweet and J. E. McCreight

Thermophysical Properties Division

Abstract

The measurements first reported by Acton on the thermal conductivity of samples taken from a borehole at the site of the proposed nuclear waste isolation pilot plant (WIPP) near Carlsbad, NM, have been extended to include additional samples and higher temperature measurements. Samples for our measurements were taken from several depths of three wells, including the well AEC 8 from which Acton obtained his samples. These samples ranged from relatively pure rocksalt (NaCl) with small amounts of interstitial anhydrite to essentially nonsalt samples composed of gypsum or clay. The measurements in this latest series were conducted at Sandia using the longitudinal heat flow apparatus described by Acton, at the Los Alamos Scientific Laboratory (LASL) using a transient line source technique, and at Dynatech Corp., Cambridge, MA using a linear heat flow comparative technique.

In general, the data from the three laboratories agreed reasonably well for similar coarse grained translucent rock salt samples, with the LASL and Sandia results typically being about 20% higher than those of Dynatech. The measured rocksalt conductivities in the temperature range 300-700 K are described relatively accurately by an expression of the form, $\lambda = \lambda_o(300/T)^\gamma$, where λ_o = conductivity at 300 K, $\gamma = 1.14$, and T is the temperature in K. The Sandia and LASL data are best described by $\lambda_o = 6$ W/m-K, while for the

Dynatech data, λ_o = 5 W/m-K yields the best fit. Slack has proposed that a two parameter expression of the form given above for λ is generally applicable to a wide variety of nonmetallic solids, with the deviation of γ from one resulting from both thermal expansion effects and optic-acoustic phonon interactions which are not included in the standard analysis of thermal conductivity caused by phonon transport. The data in the range T > 500 K frequently deviates by ~±15% from the predicted behavior. This is not believed to be the result of the onset of radiative thermal transport because the deviations are negative as well as positive. Infrared transmission measurements on rocksalt samples from the proposed WIPP site show no transmission in the 3-10 μm wavelength range for samples > 5 cm thick. Use of the estimated infrared absorption coefficient in the Rosseland radiative conductivity relation also leads to the conclusion that there is little radiative conduction for T < 800 K.

For nonsalt samples from the proposed WIPP site, values of λ_o fall in the range 0.5-3 W/m-K and frequently γ values are in the range $\gamma < 1$. All samples were dense with little or no porosity evident. On the basis of these experiments, we have concluded that the thermal conductivity of materials found at the site can be predicted to an accuracy ~±30% from knowledge of the composition and grain size of these materials.

Table of Contents

I. Introduction

The thermal conductivity measurements described in this paper were made in support of the thermal modeling studies for the proposed Waste Isolation Pilot Plant (WIPP) to be located near Carlsbad, NM. The purpose of the WIPP is to demonstrate the technology for the disposal of transuranic waste resulting from past and current U. S. defense programs. The WIPP may be converted to a waste repository after successful demonstration of the technology and a thorough assessment of repository safety for southeastern New Mexico.[1] In addition, it has been proposed that the WIPP be used as a research facility to examine the interaction between bedded salt and high-level or heat producing waste forms of various types. Ref. 1 contains an extensive discussion of the geological characterization of the area at and in the vicinity of the proposed WIPP site.

Bedded salt has long been considered an attractive choice as a storage medium for high-level or heat producing waste because of its uniformity and its relatively high thermal conductivity (~3-6 W/m-K) which facilitates heat removal from high-level power producing waste. The details of site selection and a list of references to earlier work on waste disposal in bedded salt are contained in Ref. 1. The use of salt beds for waste disposal was first discussed in detail in a National Academy of Sciences report issued in 1957.[2] Since that time an extensive literature on the subject has evolved.

The prospective high level waste experimental level is located about 800 m below the surface in a formation which is nominally composed of rocksalt or halite (NaCl). An extensive anhydrite ($CaSO_4$) bed, about 120 m thick, is located at about 860 m and a thin ≈5.5 m thick layer of anhydrite is at 730 m. As will be seen in Sec. II in the discussion of thermal conductivity measurements, the actual geologic formations or beds are quite heterogeneous

in nature. Polyhalite ($K_2Ca_2Mg(SO_4)_4 \cdot 2H_2O$) is a major "impurity" present in the salt bed formations, and the presence of this mineral can lead to a decreased thermal conductivity.

High level waste from Defense reprocessing plants is currently in temporary storage principally in the form of salts, sludges or liquid at the Savannah River Plant (SRP) near Aiken, SC; the Hanford Reservations (HR) near Richland, WA; and the Idaho National Engineering Laboratory (INEL) near Idaho Falls, ID.[3] The current reference waste canister design is a type 304-L stainless steel cylindrical canister with an outer diameter of 60 cm, a height of 2.4 m and a wall thickness of 0.53 cm. This canister would be filled with about 0.6 m^3 of waste. The power output of a waste canister depends on the waste source and the waste decay time. For times $t < 100$ y, the canister power output P_c is given relatively accurately by a relation of the form,

$$P_c(t) = P_{co} \exp(-t/\tau) \quad , \tag{1}$$

where P_{co} = 813W, 171W, and 64W for SRP, INEL and HR waste respectively, and τ = 38.95 y. Since the waste will be allowed to decay in temporary storage prior to its emplacement in a repository, the power levels will be lower than P_{co}. Typically, heat transfer calculations for SRP canisters use P_{co} = 300 W/canister.[4]

In the case of spent reactor fuel, the power output from a spent fuel assembly depends on the type of reactor, the initial enrichment, and the burnup.[3] Reactor spent-fuel waste would probably be stored in the form of fuel assemblies with one or more assemblies per canister. The highest decay heat power is produced by pressurized water reactor spent-fuel which produces $\sim 5 \times 10^3$ W/canister at $t \approx 1$ y, but then decays rapidly until $t = 15$ y, at which time P_c = 460 W/canister. For t in the range, 15 y < t < 70 y, the

decay heat power follows an expression of the form given in Eq. (1) with P_{co} = 460 W/canister, τ = 62.2 y, and t measured from the 15 y time. The numerically calculated decay heat power is given in Ref. 3. The actual volumetric power production rate will depend on the size of the spent fuel canister.

Heat sources of the sort described above produce a temperature rise in the salt formation in the vicinity of the burial site. This temperature rise can in turn produce mechanical deformations in the repository structure, with the possibility of cracks or fissures opening. It is therefore of interest to be able to predict the thermal response of the burial medium accurately, and for this prediction the thermal conductivity must be specified to some desired accuracy. It is the purpose of this paper to review a recent series of conductivity measurements made at three different laboratories, utilizing different techniques and similar samples taken from drill holes at the WIPP site. In Sec. II the measurements will be discussed and in Sec. III the experimental results will be compared with existing theory. The impact of these measurements on heat transfer calculations will be discussed in Sec. IV and conclusions of this study are presented in Sec. V.

II. Thermal Conductivity Measurements

A. Methods

The thermal conductivity of the salt specimens used in this study was measured at three different laboratories, each of which used a different technique. At Sandia Laboratories, Albuquerque, NM, the linear heat flow technique described by Acton[5] was used, while at the Los Alamos Scientific Laboratories (LASL), Los Alamos, NM, a transient line source method was employed.[6] Finally, in a recent series of measurements performed at the Dynatech Corp., Cambridge, MA, a linear heat flow thermal comparator technique was utilized.[7]

In the Sandia technique developed by Acton, a system of the type shown in Fig. 1(a) is used with a cylindrical sample of nominal dimensions 10 cm high and 10 cm in diameter. Heat is supplied from a bottom heater and flows axially up the sample and radially out the sides into a powder insulation. The system does not employ guard heaters. The centerline temperature profile is determined from thermocouples imbedded in radial holes drilled in the sample and the heat flux at the cold or top end is determined with a heat flux transducer. Further details are given in Ref. 5. The thermal conductivity is determined from the relation,

$$\lambda = \phi_z(L)/(dT/dz)_L \quad , \tag{2}$$

where $\phi_z(L)$ is the axial heat flux measured by the transducer at $z = L$ and the derivative dT/dz is calculated from a least squares polynomial fit to the $T(z_i)$ data, where the z_i are thermocouple axial locations. The advantage of this technique is that it uses a large sample which is relatively easy to machine and install in the heater apparatus. The principal disadvantage is that it is most sensitive to the conductivity at the cold end ($z = L$) and fairly insensitive to the conductivity at the other end. Hence, it will not provide an average conductivity of inhomogeneous samples but rather a conductivity which is heavily weighted by the conductivity in the region of $z = L$. Another disadvantage of the method is that it relies on the heat flux transducer calibration data supplied by the manufacturer for determination of the heat flux from the measured transducer output voltage and temperature.

The transient line source or probe method used at LASL is illustrated schematically in Fig. 1(b). A cylindrical sample is used with a heater probe installed in an axial hole drilled along the sample centerline. A temperature sensor attached to the probe measures the temperature near the probe

surface. The sample is surrounded with insulating powder and heated to a nearly uniform temperature with an external cylindrical heater. At the time t = 0 the heater probe is energized with a dc power supply, producing a constant radial heat flux characterized by a linear power density Φ(W/m) along the probe. For times t satisfying $t > a^2/4\alpha$, where a = probe radius and α = thermal diffusivity of sample, the temperature is given approximately by,[8]

$$T(a,t) = \frac{\Phi}{4\pi\lambda} [\ln(4\alpha t/a^2) - \gamma] \quad , \qquad (3)$$

where γ is Euler's constant. A plot of T(a,t) vs $\ln t$ thus has a slope $\Phi/4\pi\lambda$ from which λ may be derived. Although this technique appears to be absolute since the determination of Φ is from highly accurate measurements of the probe voltage and current, in reality end effect losses make the calculation of Φ somewhat indeterminant. As a result of this, the system is usually calibrated with a quartz specimen of known conductivity.

The comparative technique employed by Dynatech is illustrated in Fig. 1(c). A cylindrical sample of height 1.27 cm and diameter 5.1 cm with thermocouple grooves machined on the top and bottom surfaces is sandwiched between two reference disks of similar size and known conductivity with thermocouples placed in grooves along the top and bottom surfaces of each reference disk. The stack composed of sample and reference disks is sandwiched between a main and auxiliary heater and the total stack is loaded hydraulically to reduce thermal contact resistance between various stack elements. Three cylindrical guard heaters are used to minimize radial heat transport from the stack. The heat flux Φ_z through the sample is calculated as the average of the heat fluxes through the top and bottom references,

$$\Phi_z = \frac{1}{2}\left[\lambda_{r1}\Delta T_{r1}/z_{r1} + \lambda_{r2}\Delta T_{r2}/z_{r2}\right] \quad , \qquad (4)$$

where $\lambda_{r1,2}$ = conductivity of the top (1) and bottom (2) references, $\Delta T_{r1,2}$ is the temperature drop across the reference and $z_{r1,2}$ is the reference thickness. The sample conductivity is then given by

$$\lambda_s = \Phi_z/(\Delta T_s/z_s) \quad , \qquad (5)$$

where ΔT_s and z_s are the temperature drop across the sample and sample thickness respectively. The reference materials used in this investigation were Pyrex 7740 for conductivities in the range ~0.5-1.8 W/m-K and Pyroceram 9606 for conductivities in the range ~2.5-6 W/m-K. The conductivities of the reference materials were assumed to be those published by the National Bureau of Standards for these materials.

The errors inherent in the comparative technique are difficult to assess quantitatively. Measurement errors are believed to originate principally from two different sources; conductivity mismatch between reference and sample, and the presence of thermal contact resistance at the sample-reference interfaces.[9] In addition, errors in thermocouple placement can affect the accuracy of the measurement.

B. Sample Descriptions

Samples for this series of measurements were taken from three drill holes; labeled AEC#8, ERDA#9 and WIPP#19. ERDA#9 is located about 0.1 km from the center of the proposed WIPP site and in a square area approximately 0.6 km on a side designated as zone I-surface facilities area. WIPP#19 is located about 0.9 km north of ERDA#9 in an area over the prospective underground repository, and AEC#8 is located about 6 km northeast of the center and outside the WIPP site boundary. A summary of the sample descriptions is given in Table I.

Table I. Composition of WIPP Core Samples

The following composite descriptions were given by S. J. Lambert - Div. 451, Sandia Laboratories.

Core No./ Well No.	Depth (m)	Description
1/AEC#8	825	Coarse grain rocksalt with white interstitial anhydrite (~7%) with fine to coarse grain halite.
2/AEC#8	627	Medium coarse gray rocksalt; fine to very coarse halite with small pockets of gray clay (~2%) and traces of polyhalite (~1/2%).
3/ERDA#9	869	Gray very coarse crystalline rocksalt; medium to very coarse grain halite with wisps of anhydrite (~3%) and interstitial medium gray clay.
4/ERDA#9	589	Contains marker bed number 133. About 2 inches of polyhalite and very fine to coarse grain orange halite. Flesh colored polyhalite.
5/ERDA#9	590	Dense medium red fine grain polyhalite. Marker bed No. 133.
6/ERDA#9	503	Marker bed number 124. Dense gray laminated anhydrite.
7/ERDA#9	336	Medium to very coarse grain orange halite (~4%) with reddish brown clay in wispy stringers (~1%). Polyhalite associated with clay.
8/ERDA#9	607	Coarse to very coarse grain halite with anhydrite (~4%) in irregular clots and stringers, interstitial up to 2 cm long (~3%). Medium gray clay occurring as anhydrite does.
9/AEC#8MB133	610	About 8 inches of dense red polyhalite containing beds of coarse grain halite up to 2 cm thick and grading upward to very coarse grain orange halite.
10/AEC#8	609	Light orange medium to very coarse grain halite with wispy band of polyhalite (~40%) near one end.
11/AEC#8	213	Dense gray anhydrite about half converted to 50% gypsum at one end.
12/AEC#8	370	Dark red medium grain halite (~60%) and red clay (~40%).
13/AEC#8	629	Very coarse grain rocksalt with minimal clay. Traces of anhydrite and very thin line of patchy polyhalite.
14/WIPP#19	188	Dark pink medium grain laminated gypsum.
15/WIPP#19	82	Laminated cross bedded micaceous silt stone with a veinlet of gypsum parallel to bedding near the 268' level about 4 mm thick.

From an examination of Table I it can be seen that quite a variety of samples was examined.

C. Experimental Results

The results of the Dynatech and Sandia experiments are shown in Fig. 2. The top curves show results of Sandia measurements on two samples from ERDA#9. The hysteresis effect seen in the ERDA#9 630 m measurement is believed to be due to water driveoff during the heating process. The numbers on the other curves in Fig. 2 correspond to the same numbers in the first column of Table I. The majority of the samples measured had 300 K conductivities in the range ~4.5-5.5 W/m-K. For the sample with $\lambda(300\ K) < 4.5$ W/m-K (numbers 5, 9, 11, 12, 14), Table I shows that each had a substantial amount of nonsalt material, either polyhalite, clay, gypsum. The lowest conductivity measured (#14) was from a near surface sample taken from WIPP#19 at the 188 m level. It was composed entirely of laminated gypsum.

The LASL results are shown in Fig. 3 for samples from the 631 m and 799 m levels of ERDA#9. These measurements were made up to only 335 K, the upper limit of the LASL conductivity apparatus. Two samples 6.4 cm in diameter and 3.7 cm high were cut from each of the ~10 cm diameter x 20 cm high drilled blocks from each well. It can be seen that the conductivity of all of the samples exhibited about the same temperature dependence but that the magnitude of the conductivity of the two samples from the 631 m ERDA#9 core block differed by about 15%. This is quite typical of the variation which can be found in samples from nearby regions and it occurs because of local inhomogenieties in the geologic material. Also shown in Fig. 3 is a line characterized by the relation, $\lambda = 5(300/T)^{1.14}$, which represents a reasonably good fit to the Dynatech data, as will be discussed below.

For comparison purposes conductivity measurements on samples of pure granulated salt cut from a salt block furnished by the Morton Salt Co. were made at both Dynatech and Sandia. The results are shown in Fig. 4, where the Dynatech results are shown (solid line) compared to the Sandia results (dashed lines) for two different runs in which different heat flux transducers were employed. Also shown are the rocksalt conductivity results of Birch and Clark[10] which have been used extensively in the past for thermal modeling of salt repositories, and a curve (dot-dash) represented by the relation,

$$\lambda = \lambda_o(300/T)\gamma \quad , \tag{6}$$

where λ_o = 5 W/m-K and γ = 1.14. Eq. (6) represents a reasonable fit to most of the Dynatech data shown in Fig. 2 for samples composed primarily of halite and anhydrite. The Birch and Clark data can also be characterized by Eq. (6), but with λ_o = 5.5 W/m-K and γ = 1.20. The effect of variation in heat flux transducers or uncertainty in their calibration in the Sandia experiments is indicated by the shift in the Sandia data by about 25% produced by the transducer exchange.

The uncertainty in the Dynatech measurements was estimated by making a calibration run with Pyroceram 9606 as the sample and Pyrex 7740 as the reference material. The maximum observed deviation of the Pyroceram conductivity from the published NBS value was ~6% at 309 K. A 6% uncertainty is indicated by the error bar on the Dynatech data curve in Fig. 4.

III. Analysis of Results

The thermal conductivity of nonmetallic crystals has recently been discussed in detail by Slack.[11] Slack proposes a conductivity expression of the form given by Eq. (6), with the deviation of γ from unity being ascribed to

thermal expansion effects and acoustic phonon-optic phonon interactions which are not included in the basic theory.[12] From analysis of experimental data, Slack proposes λ_o = 5.9 W/m-K and γ = 1.24.[11] The NaCl conductivity data in the TPRC data series is represented quite well by λ_o = 6 W/m-K and γ = 1.16 for T > 300 K.[13] As stated in Sec. II, the Dynatech data for samples composed of salt and/or anhydrite is described well by Eq. (6) with λ_o = 5 W/m-K and γ = 1.14. The Sandia and LASL data tend to agree somewhat better with λ_o = 6 W/m-K. Measurements of anhydrite conductivity as a function of temperature have not been previously reported. A number of 293 K conductivity measurements on anhydrite samples obtained from four different locations show conductivity values in the range 4.9-5.6 W/m-K.[14]

From Fig. 2 it may be seen that $\lambda(T)$ frequently deviates from the form $\lambda(T) \propto T^{-\gamma}$ at high temperatures. These deviations are both positive and negative, with no obvious dependence on sample properties. If radiative heat transport was becoming significant at the higher temperatures, then it would be expected that the deviations would be positive, with the result that λ would be larger than the value predicted by Eq. (6). In situations where radiant transfer from the sample boundaries can be ignored in calculating the heat flux within a semitransparent solid, it can be shown that the radiant energy transfer produces a heat flux proportional to the local temperature gradient.[15] The effective conductivity is given by the Rosseland expression,

$$\lambda_R = (16/3)n^2T^3\sigma/\kappa_r \quad , \qquad (7)$$

where n = mean index of refraction, σ = Stefan-Boltzmann constant and κ_R = mean absorption coefficient as defined in Ref. 15. Using Eq. (7), an estimate may be made of the value of κ_R which will produce an appreciable value of λ_R

at 600 K, where the maximum of the blackbody spectrum occurs at a wavelength of about 5 μm. The estimate n ≈1.5 yields the relation,

$$\lambda_R(600\ K) = \frac{1.47 \times 10^2}{\kappa_R}\ W/m\text{-}K \qquad (8)$$

For λ_R to be nonnegligible, say $\lambda_R \geq 0.5$ W/m-K, Eq. (8) yields $\kappa_R \leq 300\ m^{-1}$. This limiting value of κ_R corresponds to a material with an optical thickness, $d_R \approx 5/\kappa_R \approx 1.7$ cm. The frequency averaged extinction coefficient for WIPP rocksalt has recently been measured at Sandia in the wavelength range 3.5-12.5 μm and found to fall in the range ~500-1000 m^{-1} for 0.64 cm thick samples. Although the extinction coefficient includes both scattering and absorption, it is likely that the absorption coefficient is at least an appreciable fraction of the extinction coefficient and thus the infrared transmission measurements support the conclusion that radiative conduction is not a major effect at T ≈ 600 K, but they do not absolutely rule out radiation conduction as a minor effect.

IV. Heat Transfer Analysis

The thermal conductivity plays a major role in determining the amplitude of temperature excursions in a high-level waste experiment. Analysis involving numerical solution of the heat conduction equation is used to make accurate and detailed predictions of temperatures at various points in a repository as a function of time.[4,16] However, these solutions do not show the dependence of the temperatures on the parameters such as the thermal conductivity and diffusivity. In order to demonstrate this dependence explicitly, we consider an analytic solution to the heat conduction equation for a simplified model repository geometry.

In Fig. 5(a) a simplified diagram of a portion of a high level waste burial zone is shown. Rows of canisters are buried in a "drift" region and the rows are separated by salt pillars ~25 m wide. If these discrete heat sources are smeared out in a horizontal plane, the geometry shown in Fig. 5(b) results. The temperature produced in a medium characterized by a thermal conductivity λ_s and thermal diffusivity α_s by a uniform infinite slab heat source producing a heat flux F(t) and located in the plane z = 0 is given by,[17]

$$T(z,t) = \frac{\alpha_s^{1/2}}{\lambda_s \pi^{1/2}} \int_0^t F(t-t_o) \exp(-z^2/4\alpha_s t_o) \frac{dt_o}{t_o^{1/2}} \qquad (9)$$

For an exponentially decaying heat source of the form $F(t) = F_o \exp(-t/\tau)$, Eq. (9) becomes,

$$T(z,t) = \frac{\alpha_s^{1/2} F_o e^{-t/\tau}}{\lambda_s \pi^{1/2}} \int_0^t \exp\left[t_o/\tau - z^2/4\alpha t_o\right] \frac{dt_o}{t_o^{1/2}} \qquad (10)$$

At the waste-salt interface, z = 0, the temperature is given by,

$$T(0,t) = \frac{2F_o(\alpha_s t)^{1/2}}{\lambda_s \pi^{1/2}} e^{-t/\tau} \sum_{n=0}^{\infty} \frac{1}{n!} \frac{1}{(2n+1)} \left(\frac{t}{\tau}\right)^n \qquad (11)$$

$T(0,t)$ from Eq. (11) is shown in Fig. 6 plotted as $T(0,t)/[2T_o(\alpha_s\tau)^{1/2}/\lambda_s\pi^{1/2}]$ vs t/τ. The maximum temperature occurs at $t = 0.85\tau$ and is given by

$$T_{max} = 0.54 \left[\frac{2F_o(\alpha_s\tau)^{1/2}}{\lambda_s \pi^{1/2}}\right] \qquad (12)$$

Eq. (12) exhibits a characteristic $\alpha_s^{1/2}/\lambda_s$ dependence on the thermal properties. Since $\alpha_s = \lambda_s/\rho C_p$, where ρ = mass density and C_p = specific heat per unit mass, the temperature varies as $\lambda_s^{-1/2}$, and hence a variation $\Delta\lambda_s$ in λ_s produces a corresponding variation,

$$\Delta T_{max}/T_{max} = -0.5(\Delta\lambda_s/\lambda_s) \quad . \tag{13}$$

To examine qualitatively, the magnitude of ΔT_{max}, we use the result of Sisson[4] that $T_{max} \sim 100$ K for an assumed smeared out waste areal-power density, $2F_o = 19.4$ W/m^2 (79 kW/acre). Eq. (6) predicts an average conductivity $\lambda_s = 4.3$ W/m-K for an initial temperature of 300 K and a 100 K rise in temperature. Using a typical salt density, $\rho = 2100$ kg/m^3, and specific heat, $C_p = 890$ J/kg - K, the average thermal diffusivity is calculated to be $\alpha_s = 2.3 \times 10^{-6}$ m^2/s. Using these values in Eq. (12) with $\tau = 39$ y yields the prediction, $T_{max} = 73$ K, in reasonable agreement with Sisson's numerical result. From Fig. 2, the maximum predicted conductivity variation in the high level waste burial region is $\Delta\lambda_s \sim 2.5$ W/m-K. If the conductivity was uniformly decreased by this amount, Eq. (13) yields the prediction, $\Delta T_{max} \sim 30$ K. The result shows that the largest possible variation in the maximum salt temperature is reasonably small, even for a ~60% decrease in the average salt conductivity for a homogeneous salt media.

V. Conclusions

The major conclusion of this study is that the conductivity of specimens from the proposed WIPP site which are composed predominantly of halite and/or anhydrite can be described by the expression given in Eq. (6) with λ_c in the range 4.5-5.5 W/m-K and $\gamma = 1.14$. Inclusion of significant amounts of other minerals or materials such as polyhalite, clay, or gypsum can result in

significant conductivity decreases or variations in the predicted temperature dependence. Our results on the magnitude and temperature variation of λ_s are in relatively good agreement with the results of previous rocksalt conductivity measurements. At temperatures $\gtrsim$550 K, deviations of γ_s from the prediction of Eq. (6) frequently occur. These deviations are both positive and negative, and hence our data does not confirm the predicted onset of radiative conduction in this temperature range.

The observed variation in λ_s for different samples enables a prediction of the uncertainty in value of the maximum salt temperature. For defense high level waste, the maximum temperature rise above ambient is predicted to occur about 33 y after burial and to have a magnitude in the range ~70-100 K. The uncertainty in this rise produced by a variation in the conductivity is estimated to be $\lesssim$30 K.

References

1. D. W. Powers, et al. (editors), "Geological Characterization Report, Waste Isolation Pilot Plant (WIPP) Site Southeastern New Mexico," Sandia Report, SAND 78-1596, 1978, Vols. I-II.*

2. NAS/NRC 1957 Disposal of Radioactive Wastes on Land, 1957, National Academy of Sciences - National Research Council, Washington, DC, Publ. 519.

3. S. E. Sutherland, D. E. Bennett, "Defense High-Level Waste and Spent Fuel Characterization for Geologic Waste Repositories," Sandia Report SAND 79-0172, 1979.*

4. C. E. Sisson, "Predicted Temperatures in a Bedded-Salt Repository Resulting from Burial of DOE High-Level Nuclear Waste Canisters," Sandia Report SAND-78-0924, 1978.*

5. R. E. Acton, "Thermal Conductivity of S. E. New Mexico Rocksalt and Anhydrite," in Thermal Conductivity 15, Ed. by V. V. Mirkovich (Proceedings of the 15th

International Conference on Thermal Conductivity) Plenum Press, NY, 1978, 1978, pp. 263-276.

6. J. G. Dodson, LASL, personal communication.

7. S. Spinney, "The Thermal Conductivity of Fifteen Salt Core Specimens," Dynatech R/D Co. Report No. SAD-15, contract 13-0164, 1979.

8. J. E. Parrott, A. D. Stuckes, Thermal Conductivity of Solids, Pion Ltd., London, 1975, pp. 41-42.

9. M. J. Laubitz, "Measurement of the Thermal Conductivity of Solids at High Temperatures by Using Steady-State Linear and Quasi-Linear Heat Flow," in Thermal Conductivity Vol. 1, Ed. by R. P. Tye, Academic Press, NY, 1969, pp. 174-183.

10. F. Birch, H. Clark, "The Thermal Conductivity of Rocks and Its Dependence Upon Temperature and Composition, Part II," Am. J. Sci. 238, 613 (1940).

11. G. A. Slack, "The Thermal Conductivity of Nonmetallic Crystals," in Solid State Physics Vol. 34, Ed. by F. Seitz and D. Turnbull, Academic Press, NY, 1979, pp. 1-71.

12. P. G. Klemens, "Thermal Conductivity and Lattice Vibrational Modes," in Solid State Physics Vol. VII, Ed. by F. Seitz and D. Turnbull, Academic Press Inc., NY, 1958, pp. 1-97.

13. Y. S. Touloukian, Ed., TPRC Data Series - Vol. II, Thermal Conductivity of Nonmetallic Solids, IFI/Plenum, NY, 1970, p. 621.

14. S. P. Clark, Jr. (Ed.), Handbook of Physical Constants, Geological Society of America Inc., Memoir 97, 1966, p. 463.

15. R. Viskanta, E. E. Anderson, "Heat Transfer and Semitransparent Solids," in Advances in Heat Transfer Vol II, Ed. by T. F. Irvine and J. P. Hartnett, Academic Press, NY, 1975, pp. 317-441.

16. R. D. Cheverton, W. D. Turner, "Thermal Analysis of the National Radioactive Waste Repository: Progress Through June 1971," Oak Ridge National Laboratory Report ORNL-4726, Contract No. W-7405-eng-26, Dec. 1971.*

17. H. S. Carslaw and J. C. Jaeger, Conduction of Heat in Solids, 2nd Edition, Clarendon Press, Oxford, 1959, pp. 75-76.

*Sandia and ORNL reports are available from NTIS, U. S. Dept. of Commerce, 5285 Port Royal Rd., Springfield, VA 22161.

Figure Captions

Fig. 1. (a) Sandia linear heat flow conductivity system. The conductivity is determined from a measurement of the heat flux and centerline temperature gradient at the top of the sample.

(b) LASL transient line source conductivity system. A thin center probe is inserted in a hole through the center of the cylindrical sample, and the conductivity is determined from the temperature response to a step change in heater power.

(c) Dynatech comparative thermal conductivity system. The heat flux is determined from the temperature drops across standard disks which are placed on either side of the sample. The average temperature gradient in the sample is found from measurements of sample thickness and temperature drop.

Fig. 2. Experimental conductivity vs temperature results from Dynatech (samples 1A-1B) and Sandia (ERDA#9 forward (temp. increasing) and reverse (temp. decreasing) - 630 m and ERDA#9 - 799 m).

The sample numbers correspond to the numbers in the first column of Table I.

Fig. 3. Experimental conductivity results obtained by LASL for four different samples from two different depths of well ERDA#9. Also shown is the relation, $\lambda = 5\ (300/T)^{1.14}$ which characterizes the Dynatech data.

Fig. 4. Comparison of Dynatech and Sandia data for similar samples of 99% pure granulated salt cut from a salt block furnished by the Morton Salt Co. Also shown is the data of Birch and Clark (Ref. 10) and the function given by Eq. (6) which fits the Dynatech data for WIPP rocksalt.

Fig. 5. (a) Burial scheme for waste in a high-level waste repository. Rows of canisters are buried in drift regions separated by salt pillars. The pillar spacing is determined by the maximum areal power density permitted.

(b) Smeared out heat source in the x-y plane at z = 0 producing a uniform heat flux $F_o(t)$ into each half space.

Fig. 6. Temperature vs time at the plane z = 0 produced by a heat source decaying exponentially with a half-life $t^{1/2} = 0.693\tau$. Time is measured in units of τ and temperature in units of $2F_o(\alpha_s\tau)^{1/2}/\lambda_s\pi^{1/2}$.

Figure 1.

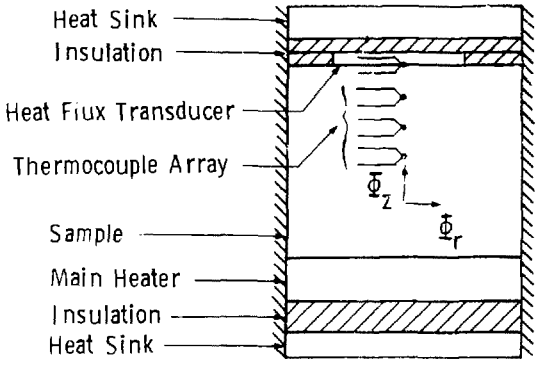

Sandia
Linear Heat Flow
Conductivity System

(a) Sandia linear heat flow conductivity system. The conductivity is determined from a measurement of the heat flux and centerline temperature gradient at the top of the sample.

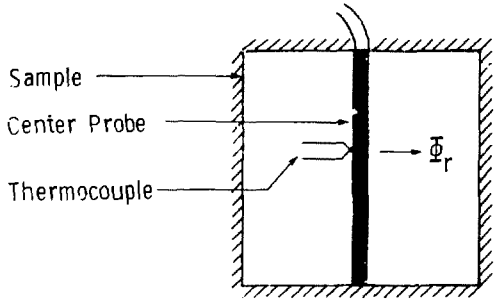

LASL
Transient Line Source
Conductivity System

(b) LASL transient line source conductivity system. A thin center probe is inserted in a hole through the center of the cylindrical sample, and the conductivity is determined from the temperature response to a step change in heater power.

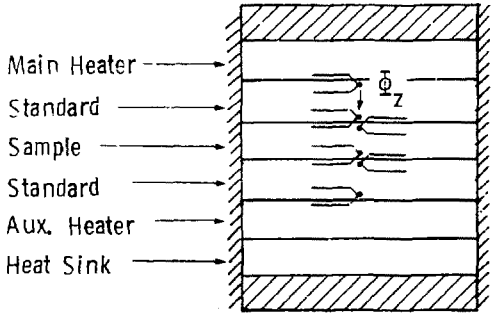

Dynatech
Comparative
Thermal Conductivity
System

(c) Dynatech comparative thermal conductivity system. The heat flux is determined from the temperature drops across standard disks which are placed on either side of the sample. The average temperature gradient in the sample is found from measurements of sample thickness and temperature drop.

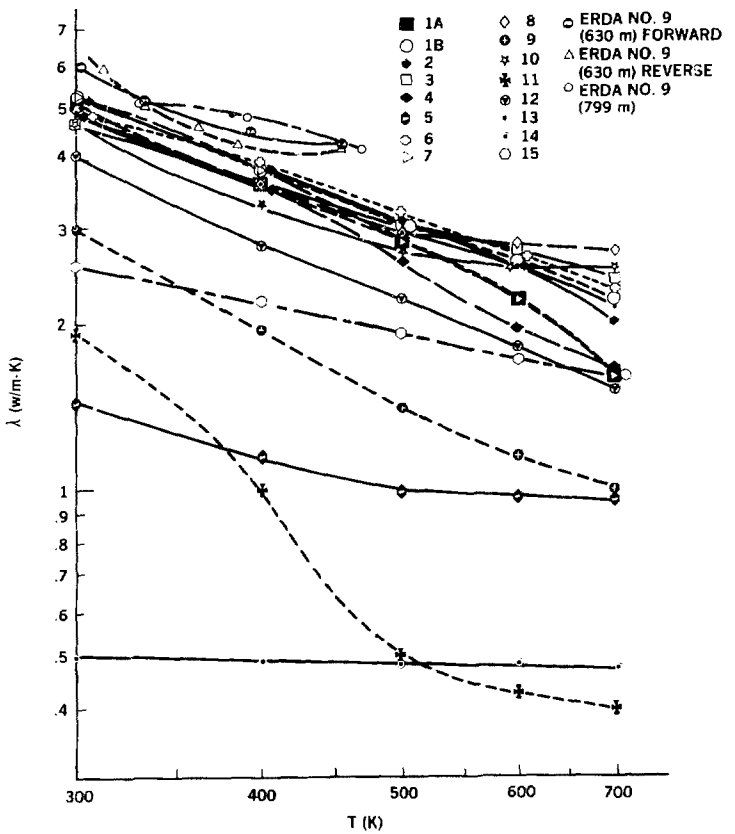

Figure 2. Experimental conductivity vs temperature results from Dynatech (samples 1A-15) and Sandia (ERDA#9 forward (temp. increasing) and reverse (temp. decreasing) - 630 m and ERDA#9 - 799 m). The sample numbers correspond to the numbers in the first column of Table I.

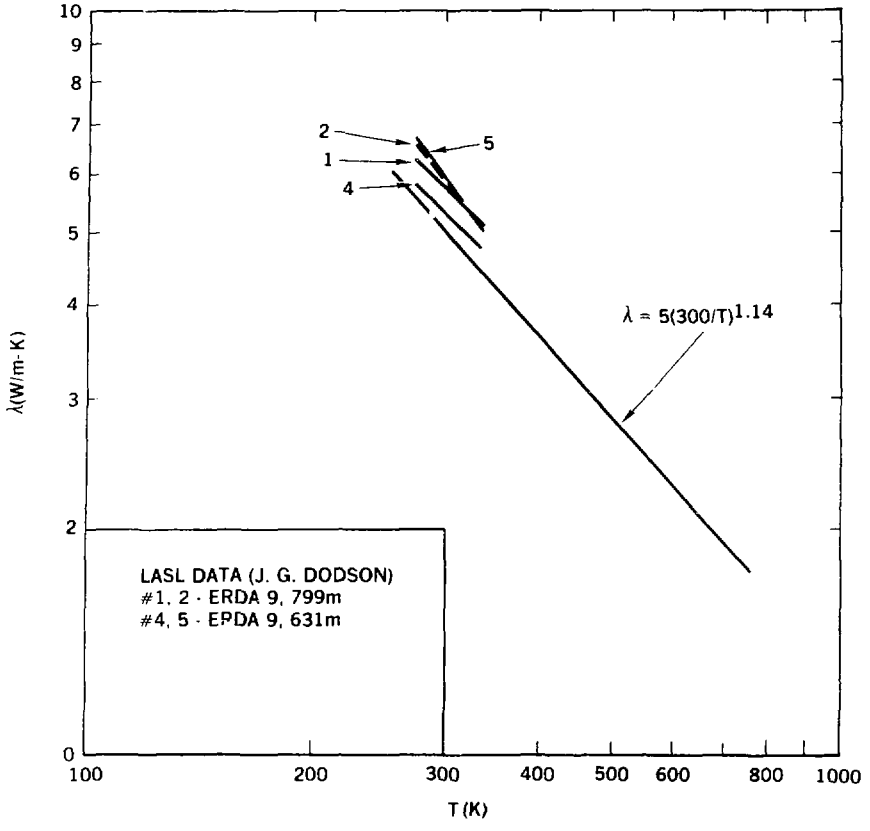

Figure 3. Experimental conductivity results obtained by LASL for four different samples from two different depths of well ERDA#9. Also shown is the relation, $\lambda = 5(300/T)^{1.14}$ which characterizes the Dynatech data.

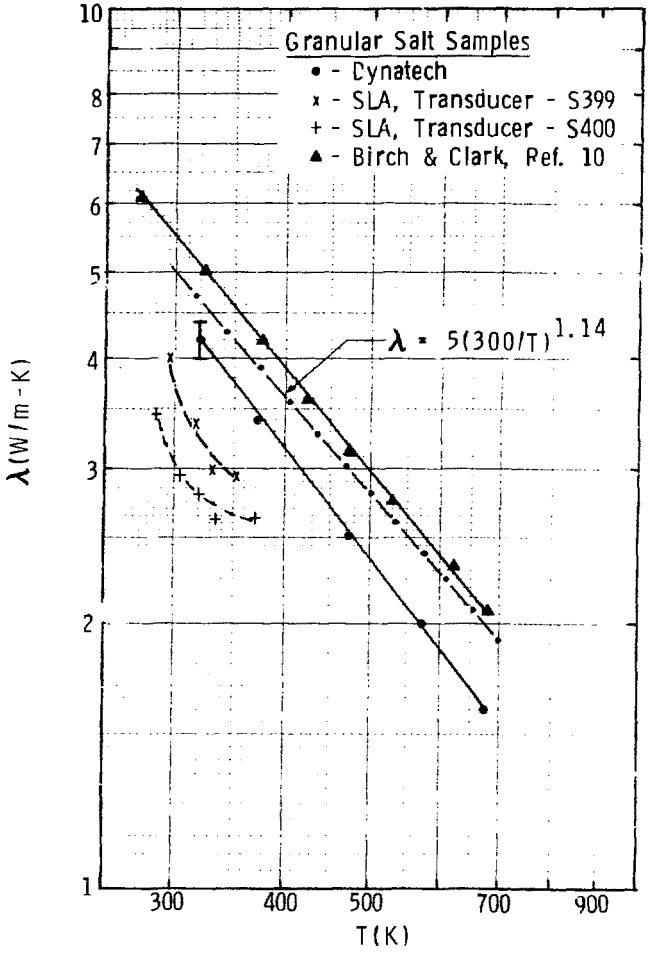

Figure 4. Comparison of Dynatech and Sandia data for similar samples of 99% pure granulated salt cut from a salt block furnished by the Morton Salt Co. Also shown is the data of Birch and Clark (Ref. 10) and the function given by Eq. (6) which fits the Dynatech data for WIPP rocksalt.

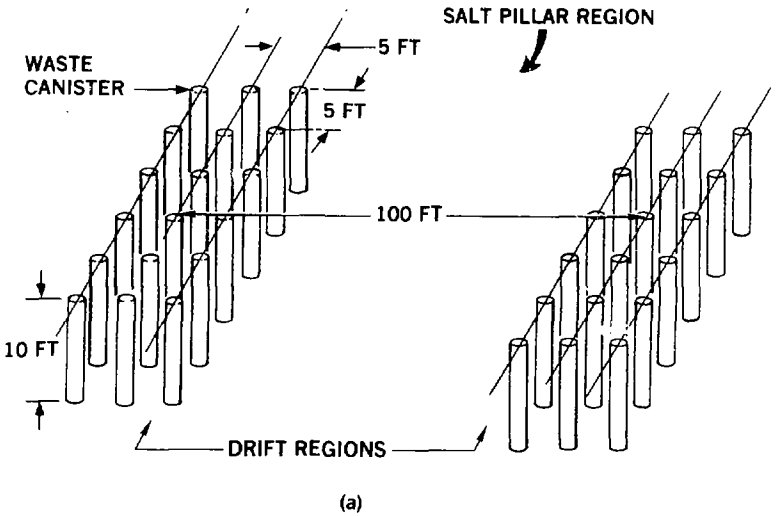

Figure 5. (a) Burial scheme for waste in a high-level waste repository. Rows of canisters are buried in drift regions separated by salt pillars. The pillar spacing is determined by the maximum areal power density permitted. (b) Smeared out heat source in the x-y plane at z = 0 producing a uniform heat flux $F_0(t)$ into each half space.

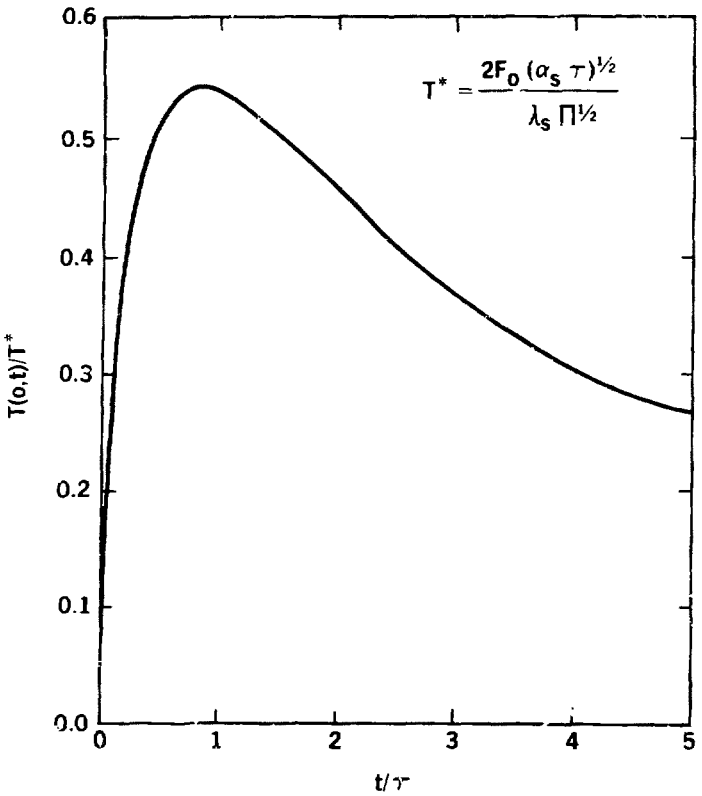

Figure 6. Temperature vs time at the plane z = 0 produced by a heat source decaying exponentially with a half-life $t^{1/2} = 0.693\tau$. Time is measured in units of τ and temperature in units of $2F_0(\alpha_s\tau)^{1/2}/\lambda_s$.

SAND 79-1665

Distribution:

U.S. Department of Energy, Headquarters
Office of Nuclear Waste Management
Washington, DC 20545
Eugene F. Beckett, Project Coordinator (WIPP) (1)
Colin A. Heath, Director, Division of Waste Isolation (2)
Sheldon Meyers
Raymond G. Romatowski
R. Stein
Carl L. Cooley
R. B. Chitwood

U.S. Department of Energy, Albuquerque Operations
P.O. Box 5400
Albuquerque, NM 87185
D. T. Schueler, Manager, WIPP Project Office (2)
R. Rudolph, Acting Deputy Manager, WIPP Project Office
G. Dennis, Director, Public Affairs Division
S. C. Taylor, C&TI Division (for Public Reading Rooms)
J. F. Bresson
G. W. Johnson, Waste Management Branch

U.S. Department of Energy
Carlsbad WIPP Project Office
Room 113, Federal Building
Carlsbad, NM 88220

U.S. Department of Energy
c/o Battelle
Office of Nuclear Waste Isolation
505 King Avenue
Columbus, OH 43201
Jeff O. Neff

Battelle Memorial Institute
Office of Nuclear Waste Isolation
505 King Avenue
Columbus, OH 43201
Neil Carter, General Manager (3)
R. Heineman
Wayne Carbiener
P. Hoffman
A. A. Bauer

Westinghouse Electric Corporation
P.O. Box 40039
Albuquerque, NM 87196
R. C. Mairson
D. Hulbert
V. F. Likar
H. H. Irby
A. K. Kuhn, D'Appolonia

National Academy of Sciences
Committee on Radioactive Waste Management
2101 Constitution Avenue
Washington, DC 20418
J. Holloway (2)

Hobbs Public Library
509 N. Ship Street
Hobbs, NM 88248
Ms. Marcia Lewis, Librarian

Lokesh Chaturvedi
Department of Civil Engineering
Box 3E
New Mexico State University
Las Cruces, NM 88003

Bechtel Inc.
P. O. Box 3965
San Francisco, CA 94119
R. A. Langley
H. G. Taylor
D. L. Roberts
D. Duncan

National Academy of Sciences, WIPP Panel
Frank L. Parker, Chairman
Department of Environmental and
Water Resources Engineering
Vanderbilt University
Nashville, TN 37235

Konrad B. Krauskopf, Vice Chairman
Department of Geology
Stanford University
Stanford, CA 94305

Neville G. W. Cook, Member
Dept. of Material Sciences and Engineering
University of California at Berkeley
Heart Mining Building, #320
Berkeley, CA 94720

Merril Eisenbud, Member
Inst. of Environmental Medicine
New York University Medical Center
Box 817
Tuxedo, NY 10987

Fred M. Ernsberger, Member
Glass Research Center
PPG Industries, Inc.
Box 11472
Pittsburgh, PA 15238

Roger Kasperson, Member
Center for Technology, Environment and Development
Clark University
Worcester, MA 01610

Richard R. Parizek, Member
Department of Hydrogeology
Pennsylvania State University
University Park, PA 16802

Thomas H. Pigford, Member
Department of Nuclear Engineering
University of California
Berkeley, CA 94720

National Academy of Sciences, WIPP Panel

Roger W. Staehle, Member
Dean, Institute of Technology
University of Minnesota
Lind Hall
Minneapolis, MN 55455

John W. Winchester, Member
Department of Oceanography
Florida State University
Tallahassee, FL 32306

D'Arcy A. Shock, Consultant
233 Virginia
Ponca City, OK 74601

John T. Holloway, Executive Secretary
2101 Constitution Avenue, NW
Washington, DC 20418

WIPP Public Reading Room
Atomic Museum, Kirtland East AFB
Albuquerque, NM 87185
Ms. Gwynn Schreiner

WIPP Public Reading Room
Carlsbad Municipal Library
101 S. Hallagueno St.
Carlsbad, NM 88220
Lee Hubbard, Head Librarian

Thomas Brannigan Library
106 W. Hadley St.
Las Cruces, NM 88001
Don Dresp, Head Librarian

Roswell Public Library
301 N. Pennsylvania Avenue
Roswell, NM 88201
Ms. Nancy Langston

Dr. Bruno Giletti, Co-Chairman
Department of Geological Sciences
Brown University
Providence, Rhode Island 02912

Dr. Raymond Siever, Co-Chairman
Department of Geological Sciences
Harvard University
Cambridge, Massachusetts 02138

Dr. John Handin, Director
Center of Tectonophysics
Texas A & M University
College Station, Texas 77840

Dr. John Lyons
Department of Earth Sciences
Dartmouth College
Hanover, New Hampshire 03755

Dr. George Pinder
Department of Civil Engineering
Princeton University
Princeton, New Jersey 08540

New Mexico Advisory Committee on WIPP
NMIMT Graduate Office
Socorro, NM 87801
Marvin H. Wilkening, Chairman (2)

State of New Mexico
Environmental Evaluation Group
720 Marcy Street
P.O. Box 968
Santa Fe, NM 87503
Robert H. Neill, Director (2)

NM Department of Energy & Minerals
P. O. Box 2770
Santa Fe, NM 87501
Larry Kehoe, Secretary
Kasey LaPlante, Librarian

J. E. Magruder
Sandia Carlsbad Representative
401 North Canal Street
Carlsbad, NM 88220

Paul W. Levy
Physics Department
Brookhaven National Laboratory
Associated Universities, Inc.
Upton, Long Island, New York 11973

Sandia Internal:
3141 T. L. Werner (5)
3151 W. L. Garner, for: DOE/TIC (Unlimited Release) (3)
3154-3 R. P. Campbell, for: DOE/TIC (25)
4500 E. H. Beckner
4510 W. D. Weart
4511 W. D. Weart (Acting)
4512 T. O. Hunter (5)
4512 C. L. Christensen
4512 D. R. Fortney
4512 M. A. Molecke
4514 M. L. Merritt
4522 R. W. Lynch
4540 M. L. Kramm
4541 L. W. Scully
4542 Sandia WIPP Central File, (2) (TS1)
4732 D. E. Munson
5510 D. B. Hayes
5511 J. W. Nunziato
5511 D. F. McVey
5511 G. R. Hadley
5521 S. W. Key
5530 W. Herrmann
5531 L. D. Bertholf
5532 B. M. Butcher
5800 R. S. Claassen
Attn: 5810 R. G. Kepler
5830 M. J. Davis
5840 N. J. Magnani
5820 R. E. Whan
5824 J. N. Sweet (4)
5824 J. E. McCreight (2)
5824 J. A. Koski
5824 M. Moss
8310 D. M. Schuster
8266 E. A. Aas (1)